
Strain Smoothing for Stabilization and Regularization of Galerkin Meshfree Methods

J. S. Chen¹, W. Hu¹, M. Puso², Y. Wu¹, and X. Zhang¹

¹ Department of Civil & Environmental Engineering
University of California, Los Angeles
Los Angeles, CA 90095, USA
jschen@seas.ucla.edu

² Department of Mechanical Engineering
Lawrence Livermore National Laboratory
Livermore CA 94550, USA

Summary. In this paper we introduce various forms of strain smoothing for stabilization and regularization of two types of instability: (1) numerical instability resulting from nodal domain integration of weak form, and (2) material instability due to material strain softening and localization behavior. For numerical spatial instability, we show that the conforming strain smoothing in stabilized conforming nodal integration only suppresses zero energy modes resulting from nodal domain integration. When the spurious nonzero energy modes are excited, additional stabilization is proposed. For problems involving strain softening and localization, regularization of the ill-posed problem is needed. We show that the gradient type regularization method for strain softening and localization can be formulated implicitly by introducing a gradient reproducing kernel strain smoothing. It is also demonstrated that the gradient reproducing kernel strain smoothing also provides a stabilization to the nodally integrated stiffness matrix. For application to modeling of fragment penetration processes, a nonconforming strain smoothing as a simplification of conforming strain smoothing is also introduced.

Key words: Strain smoothing, Stabilization, Regularization, Meshfree, Nodal integration

1 Introduction

Nodal integration offers considerable efficiency in Galerkin type meshfree methods, but it encounters spatial instability due to under integration and vanishing derivatives of meshfree shape functions at nodes. Several methods have been introduced as a correction and stabilization of nodal integration. Beissel et al. [1] proposed a least-squares stabilization technique. Randles et al. [12] introduced stress point method to enhance collocation formulation for

SPH. Bonet et al. [2] presented a correction term into the derivative of shape function at nodal point, which is constructed by satisfying a linear patch test. Chen et al. [5, 6, 13, 14] proposed a conforming strain smoothing in a stabilized conforming nodal integration (SCNI) as a stabilization of rank instability in nodal integration, and as a mechanism to pass linear patch test. Our recent study showed that SCNI produces spurious low energy modes under certain conditions. A modified SCNI is introduced, and its stability in reproducing kernel particle method is examined. For application to modeling of fragment penetration processes, a nonconforming strain smoothing as a simplification of conforming strain smoothing is also introduced.

Material instability refers to the event of strain softening and localization that yields an ill-posed problem. The difficulty in strain localization arises because solutions possess features of measure zero, and as such, characteristic length of the mesh introduces a mesh-size perturbation. The dependence on the discretization is not only with respect to mesh refinement but is also with respect to the mesh alignment. The inability of the classical continuum theory to describe the discontinuous strain fields can be corrected if the discontinuous strain field is regularized (smoothed). A commonly used regularization method in strain localization is the gradient method [8, 9, 10]. The classical gradient type regularization results in a governing equation with higher order differentiation, and thus requires additional nonphysical boundary conditions for a solution. A gradient reproducing kernel strain smoothing has been introduced as a regularization of strain localization problem [7, 4]. This gradient type regularization can be implicitly imbedded in a reproducing kernel approximation of strain, and thus does not require additional nonphysical boundary conditions to solve the regularized governing equation. In this work, we show that this gradient strain smoothing offers a stabilization of nodally integrated stiffness matrix similar to the one-point integrated stiffness with stabilization obtained from Taylor expansion of gradient matrix in the finite element setting [11].

This paper is organized as follows. In Section 2, we review the conforming strain smoothing in the stabilized conforming nodal integration (SCNI) for rank instability. In Section 3, we show that SCNI only eliminates improper zero energy modes, and additional stabilization is introduced to suppress spurious nonzero energy modes. In Section 4, we first demonstrate how gradient type regularization method for strain localization can be formulated under a gradient reproducing kernel strain smoothing. The eigenmodes associated with the regularized weak form integrated by nodal integration are also examined. For application to fragment problems in Section 5, we introduce a nonconforming strain smoothing as a simplification of conforming strain smoothing in SCNI. Concluding remarks are given in Section 6.

2 Conforming Strain Smoothing for Rank Instability

Domain integration of weak form poses considerable complexity in Galerkin meshfree method. Employment of Gauss quadrature rules yields integration error when background grids do not coincide with the covers of shape functions. Nodal integration, on the other hand, results in rank deficiency. Further, both Gauss integration and nodal integration methods do not pass linear patch test for nonuniform point distribution. For demonstration of rank instability, consider the following Poisson problem with Dirichlet boundary condition:

$$\nabla^2 u + Q = 0 \text{ in } \Omega \quad (1)$$

By introducing test function v^h , the corresponding Galerkin approximation is

$$a(v^h, u^h) = (v^h, Q) \quad (2)$$

By introducing nodal integration we have the following discrete bilinear form associated with the differential operator:

$$a^h(v^h, u^h) = \sum_{L=1}^N \nabla v^h(\mathbf{x}_L) \cdot \nabla u^h(\mathbf{x}_L) w_L \quad (3)$$

where w_L is the weight associated with point L . A rank instability resulting from nodal integration in (3) is shown in figure 1 (a), where the test and trial functions are approximated by reproducing kernel approximation with linear basis. Low convergence rate in nodal integration is also observed in figure 1 (b).

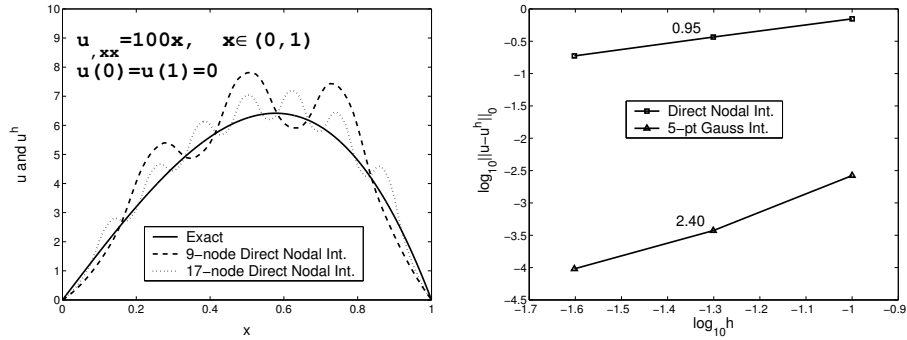


Figure 1. Nodal integration of weak form yields (a) rank instability (b) low convergence rate.

It is shown in figure 1, even when the approximation of test and trial functions is linearly complete, the first order accuracy is not guaranteed in the Galerkin approximation due to nodal integration. Integration constraints are necessary

conditions for linear exactness in the Galerkin approximation [5]. There are two requirements for linear exactness in the Galerkin approximation of second order differential equations. The first condition requires the approximation functions $\Psi_I(\mathbf{x})$ of u^h and v^h to possess linear consistency:

$$\sum_{I=1}^{NP} \Psi_I(\mathbf{x}) = 1, \quad \sum_{I=1}^{NP} \Psi_I(\mathbf{x}) \mathbf{x}_I = \mathbf{x} \quad (4)$$

These conditions are automatically satisfied in the reproducing kernel shape functions $\Psi_I(\mathbf{x})$ if complete linear bases are used. The second condition requires the numerical integration to satisfy the following integration constraint [5]:

$$\int_{\Omega}^{\wedge} \nabla \Psi_I d\Omega = \int_{\partial\Omega}^{\wedge} \Psi_I \mathbf{n} d\Gamma \quad (5)$$

where \int^{\wedge} denotes numerical integration. A stabilized conforming nodal integration (SCNI) [5] has been introduced to satisfy linear patch test and to remedy rank instability of nodal integration. In SCNI approach, a conforming smoothed gradient operator at nodal point \mathbf{x}_L is introduced as

$$\bar{\nabla} u^h(\mathbf{x}_L) = \sum_I \bar{\nabla} \Psi_I(\mathbf{x}_L) d_I \quad (6)$$

$$\bar{\nabla} \Psi_I(\mathbf{x}_L) = \frac{1}{w_L} \int_{\Omega_L} \nabla \Psi_I d\Omega = \frac{1}{w_L} \int_{\partial\Omega_L} \Psi_I \mathbf{n} d\Gamma, \quad w_L = \int_{\Omega_L} d\Omega \quad (7)$$

Here Ω_L is the nodal representative domain, which can be obtained from triangulation or Voronoi cell of a set of discrete points as shown in figure 2. Note that a divergence theorem has been used in (7) to pass linear patch test when the weak form is integrated by nodal integration. It can be easily shown that the conforming smoothed gradient satisfies integration constraint of (5) using nodal integration, i.e.,

$$\begin{aligned}
 \int_{\Omega} \hat{\nabla} \Psi_I d\Omega &= \sum_{L=1}^{NP} \bar{\nabla} \Psi_I(\mathbf{x}_L) w_L \\
 &= \sum_{L=1}^{NP} \left(\frac{1}{w_L} \int_{\partial\Omega_L} \Psi_I \mathbf{n} d\Gamma \right) w_L \\
 &= \sum_{L=1}^{NP} \int_{\partial\Omega_L} \Psi_I \mathbf{n} d\Gamma \\
 &= \int_{\partial\Omega} \Psi_I \mathbf{n} d\Gamma
 \end{aligned} \tag{8}$$

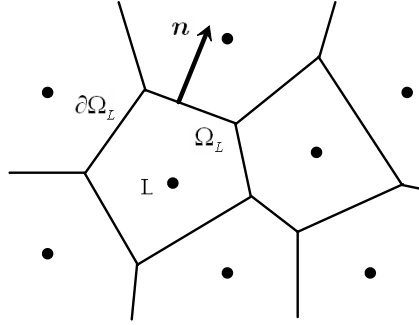


Figure 2. Nodal representative domains.

Note that to yield the results of (8) we have used the conforming property of nodal representation domain Ω_L as shown in figure 2. Introducing the smoothed gradient of (7) into (3) yields the following discrete differential operator:

$$\bar{a}^h(v^h, u^h) = \sum_{L=1}^{NP} \bar{\nabla} v^h(\mathbf{x}_L) \cdot \bar{\nabla} u^h(\mathbf{x}_L) w_L \tag{9}$$

The corresponding stiffness matrix is

$$\mathbf{K}_{IJ} = \sum_{L=1}^{NP} \bar{\mathbf{B}}_I^T(\mathbf{x}_L) \bar{\mathbf{B}}_J(\mathbf{x}_L) w_L$$

$$\bar{\mathbf{B}}_I(\mathbf{x}_L) = \frac{1}{w_L} \int_{\partial\Omega_L} \Psi_I \mathbf{n} d\Gamma$$

$$w_L = \int_{\Omega_L} d\Omega \quad (10)$$

The problem in figure 1 is solved again for comparison of solution of using SCNI, nodal integration, and the fifth order Gauss quadrature rule as shown in figure 3.

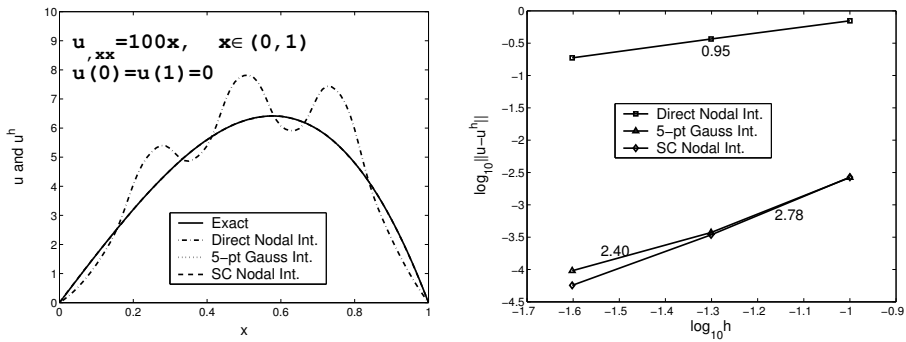


Figure 3. Comparison of solution obtained from various domain integration methods.

3 Additional Stabilization for Spurious Nonzero Energy Modes

The spurious zero energy mode with alternating gradient generates zero smoothed gradient at nodal point, except on the boundary. Thus for a finite domain, zero energy modes cannot propagate as the nonzero smoothed gradient on the boundary precludes the zero energy mode. However, the energy of an oscillatory mode can be very small and stability is not ensured as the mesh is refined. The V_1 coercivity requires the following condition for any non rigid body modes:

$$a^h(v^h, u^h) \geq \gamma \|u^h\|_1^2 \quad (11)$$

where γ is a mesh independent constant. Consider a uniform discretization of a one-dimensional domain by $N + 1$ uniformly distributed points, and let

the nodal value of u to take the oscillating pattern $[+1, -1, +1, \dots, +1, -1]$ we have the following bilinear form of SCNI with smoothed gradient:

$$\begin{aligned} \bar{a}^h(v^h, u^h) &= \frac{h}{2} \left(\frac{u_2 - u_1}{h} \right)^2 + h \left(\frac{u_3 - u_1}{2h} \right)^2 + \dots + \\ &\quad + h \left(\frac{u_{N+1} - u_{N-1}}{2h} \right)^2 + \frac{h}{2} \left(\frac{u_{N+1} - u_N}{h} \right)^2 \\ &= \frac{4}{h} \end{aligned} \quad (12)$$

where h is the nodal distance. It can also be shown

$$\begin{aligned} \|u^h\|_1^2 &= \int_0^L u^2 dx + \int_0^L u_{,x}^2 dx \\ &= \frac{1}{3} (u_1^2 + u_1 u_2 + u_2^2) h + \frac{1}{3} (u_2^2 + u_2 u_3 + u_3^2) h + \dots + \\ &\quad + \frac{1}{3} (u_N^2 + u_N u_{N+1} + u_{N+1}^2) h + \left(\frac{u_2 - u_1}{h} \right)^2 h + \\ &\quad + \left(\frac{u_3 - u_2}{h} \right)^2 h + \dots + \left(\frac{u_{N+1} - u_N}{h} \right)^2 h \\ &= \frac{1}{3} L + \frac{4}{h^2} L \\ &= \frac{h^2 + 12}{3h^2} L \end{aligned} \quad (13)$$

It follows $\gamma = \bar{a}^h(v^h, u^h) / \|u^h\|_1^2 = \frac{12h}{L(h^2+12)} \rightarrow 0$ as $h \rightarrow 0$ and thus violating coercivity. One way to gain coercivity in SCNI is to consider the following modification:

$$\begin{aligned} &\bar{a}^h(v^h, u^h) \\ &= \sum_{L=1}^{NP} \left\{ \underbrace{\bar{\nabla} v^h(\mathbf{x}_L) \cdot \bar{\nabla} u^h(\mathbf{x}_L)}_{\text{SCNI}} + \right. \\ &\quad \left. + \underbrace{\sum_{K \in S_L} [c_L^K ((\nabla v^h)_L^K - \bar{\nabla} v^h(\mathbf{x}_L)) \cdot ((\nabla u^h)_L^K - \bar{\nabla} u^h(\mathbf{x}_L))]}_{\text{Additional stabilization}} \right\} w_L \end{aligned} \quad (14)$$

where $(\nabla u^h)_L^K$ is ∇u^h evaluated at the centroid of the K -th Delaunay triangles associated with node L as shown in figure 4, c_L^K is the stabilization parameter, and S_L is the set containing Delaunay triangles associated with node L .

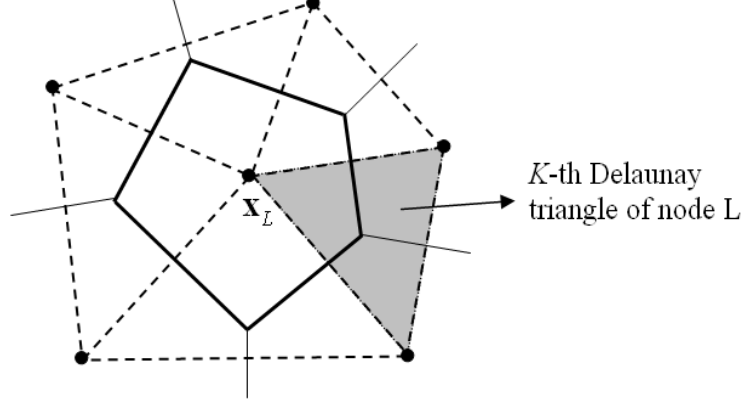


Figure 4. Voronoi cell and Delaunay triangulation.

In elasticity, the Galerkin approximation is

$$a(\mathbf{v}^h, \mathbf{u}^h) = (\mathbf{v}^h, \mathbf{b}) + (\mathbf{v}^h, \mathbf{h})_{\partial\Omega^{h_i}} \quad (15)$$

where $(\mathbf{v}^h, \mathbf{b})$ and $(\mathbf{v}^h, \mathbf{h})_{\partial\Omega^{h_i}}$ are the standard linear forms in domain Ω and Neumann boundary $\partial\Omega^{h_i}$, respectively, \mathbf{b} is the body force vector, \mathbf{h} is the traction vector, and $a(\mathbf{v}^h, \mathbf{u}^h)$ in elasticity is

$$a(\mathbf{v}^h, \mathbf{u}^h) = \int_{\Omega} \nabla^s \mathbf{v}^h : \mathbf{C} : \nabla^s \mathbf{u}^h d\Omega \equiv \int_{\Omega} \boldsymbol{\varepsilon}(\mathbf{v}^h) : \mathbf{C} : \boldsymbol{\varepsilon}(\mathbf{u}^h) d\Omega \quad (16)$$

where

$$\boldsymbol{\varepsilon}(\mathbf{u}^h)_{ij} \equiv (\nabla^s \mathbf{u}^h)_{ij} = \frac{1}{2} \left(\frac{\partial u_i^h}{\partial x_j} + \frac{\partial u_j^h}{\partial x_i} \right) \quad (17)$$

and \mathbf{C} is the 4-th rank elasticity tensor. By taking a similar modified SCNI procedure with smoothed gradient on ∇^s , we have the following discrete equation:

$$\bar{a}^h(\mathbf{v}^h, \mathbf{u}^h) = (\mathbf{v}^h, \mathbf{b})^h + (\mathbf{v}^h, \mathbf{h})_{\partial\Omega^{h_i}}^h \quad (18)$$

Here $(\mathbf{v}^h, \mathbf{b})^h$ and $(\mathbf{v}^h, \mathbf{h})_{\partial\Omega^h}^h$ are obtained by nodal integration, and

$$\begin{aligned}
 & \bar{a}^h(\mathbf{v}^h, \mathbf{u}^h) \\
 &= \sum_{L=1}^{NP} \left\{ \underbrace{\bar{\varepsilon}(\mathbf{v}^h)_L : \mathbf{C} : \bar{\varepsilon}(\mathbf{u}^h)_L}_{\text{SCNI}} + \right. \\
 & \left. + \underbrace{\sum_{K \in S_L} \left[c_L^K \left(\varepsilon(\mathbf{v}^h)_L^K - \bar{\varepsilon}(\mathbf{v}^h)_L \right) : \mathbf{C} : \left(\varepsilon(\mathbf{u}^h)_L^K - \bar{\varepsilon}(\mathbf{u}^h)_L \right) \right]}_{\text{Additional stabilization}} \right\} w_L
 \end{aligned} \tag{19}$$

where

$$\begin{aligned}
 (\bar{\varepsilon}(\mathbf{u}^h)_L)_{ij} &= \frac{1}{w_L} \int_{\hat{\Omega}_L} \frac{1}{2} \left(\frac{\partial u_i^h}{\partial x_j} + \frac{\partial u_j^h}{\partial x_i} \right) d\Omega \\
 &= \frac{1}{w_L} \int_{\partial\hat{\Omega}_L} \frac{1}{2} (\partial u_i^h n_j + \partial u_j^h n_i) d\Gamma \\
 &= \sum_{I=1}^{NP} \frac{1}{2} (\bar{\nabla}_i \Psi_I d_{jI} + \bar{\nabla}_j \Psi_I d_{iI})
 \end{aligned} \tag{20}$$

$$\bar{\nabla}_i \Psi_I = \frac{1}{w_L} \int_{\partial\hat{\Omega}_L} \Psi_I n_i d\Gamma, \tag{21}$$

and $\varepsilon(\mathbf{u}^h)_L^K$ is $\varepsilon(\mathbf{u}^h)$ evaluated at the centroid of the K -th Delaunay triangles associated with node L as shown in figure 4, and c_L^K is the stabilization parameter.

A first nonzero eigenmode associated with the stiffness in two dimensional elasticity ($E = 1, \nu = 0.499$) integrated using SCNI is shown in figure 5. The corresponding eigenvalue of this mode is 0.0211. The first nonzero energy eigenmode obtained using modified SCNI (M-SCNI) with stabilization parameter $c_L^K = c = 0.01$, which will be used for all the following numerical examples, has shown to provide stabilization.

A cantilever beam shown in figure 6 is analyzed. Figure 7 compares the results of SCNI and M-SCNI with different stabilization parameters c . It is shown that the use of $c = 0.01$ in M-SCNI that properly suppresses spurious nonzero

energy modes in figure 5 also generates good convergence rate in figure 7.

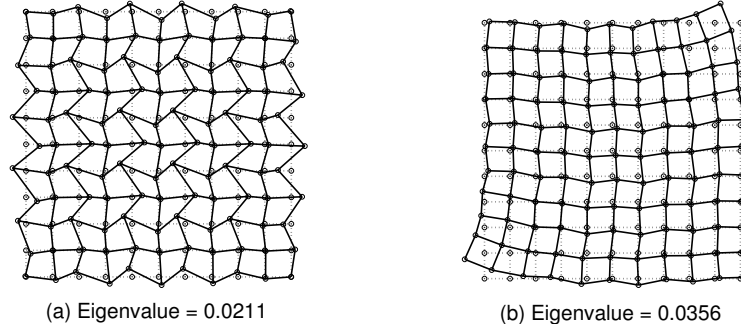


Figure 5. First nonzero energy eigenmode generated using (a) SCNI and (b) M-SCNI with $c = 0.01$.

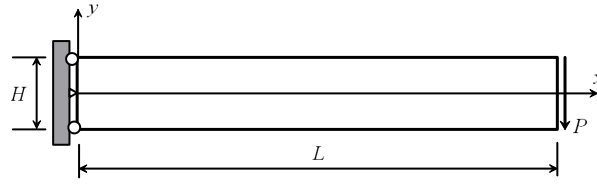


Figure 6. Cantilever beam ($L = 10m$, $H = 2m$, $P = 200N$, $E = 3 \times 10^7 Pa$, $\nu = 0.25$).

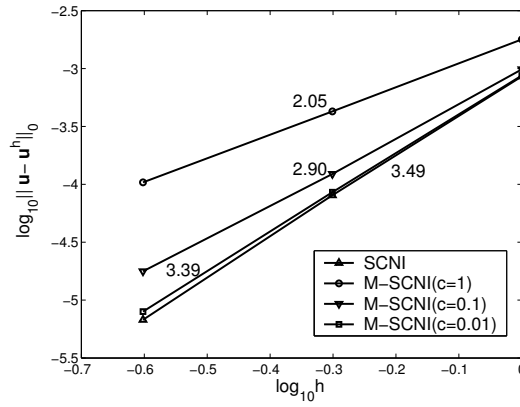


Figure 7. Convergence rate of L_2 error norm.

The numerical studies show that the use of a minimum value in $c_L^K = c = 0.01$ is required for stability. Employment of c_L^K larger than 0.01, on the other hand, yields reduction of convergence rate. It is recommended that $c_L^K = c = 0.01$ be employed in M-SCNI for stability and accuracy.

4 Gradient Strain Smoothing Regularization for Material Instability in Strain Localization

Strain localization is usually a precursor of catastrophic material failure. In the event of strain softening and localization, the change of sign in the tangent moduli yields an ill-posed problem and requires a regularization for unique solution. A commonly used regularization method in strain localization is the gradient method [8, 9, 10], where a "nonlocal strain" $\tilde{\varepsilon}$ is introduced as

$$\tilde{\varepsilon}(\mathbf{x}) = \varepsilon(\mathbf{x}) + \sum_{i+j=1}^n \beta_{ij} D_{ij} \varepsilon(\mathbf{x}) \quad (22)$$

where ε is any component of strain, and $D_{ij}(\cdot) = \partial^{i+j}(\cdot)/\partial x_1^i \partial x_2^j$. However, introducing strain regularization of (22) into equilibrium equation leads to a PDE with higher order differentiation and thus requires additional non-physical boundary conditions to solve the problem. Until now, the physical explanation of these additional boundary conditions is still lacking [9]. The issue of additional boundary conditions has been addressed by introducing a gradient reproducing kernel strain smoothing [4, 7] as follows:

$$\tilde{\varepsilon}(\mathbf{x}) = \int_{\Omega} \tilde{\Phi}_a(\mathbf{x}; \mathbf{x} - \mathbf{s}) \varepsilon(\mathbf{s}) d\mathbf{s} \quad (23)$$

We write the discrete counter part of the strain smoothing equation as

$$\tilde{\varepsilon}(\mathbf{x}) = \sum_{I=1}^{NP} \tilde{\Phi}_a(\mathbf{x}; \mathbf{x} - \mathbf{x}_I) \varepsilon(\mathbf{x}_I) \quad (24)$$

where $\tilde{\Phi}_a(\mathbf{x}; \mathbf{x} - \mathbf{x}_I)$ is a smoothing function that takes the following reproducing kernel form:

$$\begin{aligned} \tilde{\Phi}_a(\mathbf{x}; \mathbf{x} - \mathbf{x}_I) &= \left[\sum_{i+j=0}^n (x_1 - x_{1I})^i (x_2 - x_{2I})^j b_{ij}(\mathbf{x}) \right] \Phi_a(\mathbf{x} - \mathbf{x}_I) \\ &\equiv \mathbf{H}^T(\mathbf{x} - \mathbf{x}_I) \mathbf{b}(\mathbf{x}) \Phi_a(\mathbf{x} - \mathbf{x}_I) \end{aligned} \quad (25)$$

The vector $\mathbf{b}(\mathbf{x})$ is obtained by imposing the following gradient reproducing conditions according to the gradient regularization equation (22):

$$\sum_{I=1}^{NP} x_{1I}^p x_{2I}^q \tilde{\Phi}_a(\mathbf{x}; \mathbf{x} - \mathbf{x}_I) = x_1^p x_2^q + \sum_{i+j=0}^n \beta_{ij} D_{ij}(x_1^p x_2^q) \quad (26)$$

$$0 \leq p + q \leq n, \quad \beta_{00} = 0$$

It can be shown that the above equation is equivalent to

$$\sum_{I=1}^{NP} (x_1 - x_{1I})^p (x_2 - x_{2I})^q \tilde{\Phi}_a(\mathbf{x}; \mathbf{x} - \mathbf{x}_I) = \delta_{p0} \delta_{q0} + \beta_{pq} (-1)^{p+q} p! q! \quad (27)$$

$$0 \leq p + q \leq n, \quad \beta_{00} = 0$$

This leads to a system of discrete equations for $\mathbf{b}(\mathbf{x})$

$$\mathbf{M}(\mathbf{x}) \mathbf{b}(\mathbf{x}) = \mathbf{g} \quad (28)$$

where \mathbf{g} is the vector form of $g_{ij} = \delta_{i0} \delta_{j0} + \beta_{ij} (-1)^{i+j} i! j!$, and

$$\mathbf{M}(\mathbf{x}) = \sum_{I=1}^{NP} \mathbf{H}(\mathbf{x} - \mathbf{x}_I) \mathbf{H}^T(\mathbf{x} - \mathbf{x}_I) \Phi_a(\mathbf{x} - \mathbf{x}_I) \quad (29)$$

Substituting $\mathbf{b}(\mathbf{x}) = \mathbf{M}^{-1}(\mathbf{x}) \mathbf{g}$ into (25), we obtain the following strain smoothing function

$$\tilde{\Phi}_a(\mathbf{x}; \mathbf{x} - \mathbf{x}_I) = \mathbf{H}(\mathbf{x} - \mathbf{x}_I) \mathbf{M}^{-1}(\mathbf{x}) \mathbf{g} \Phi_a(\mathbf{x} - \mathbf{x}_I) \quad (30)$$

Due to the employment of gradient reproducing conditions in the construction of smoothing function $\tilde{\Phi}_a$, we have the following property:

$$\tilde{\varepsilon}(\mathbf{x}) = \sum_{I=1}^{NP} \tilde{\Phi}(\mathbf{x}; \mathbf{x} - \mathbf{x}_I) \varepsilon(\mathbf{x}_I) \approx \varepsilon(\mathbf{x}) + \sum_{i+j=1}^n \beta_{ij} D_{ij} \varepsilon(\mathbf{x}) \quad (31)$$

For example, in one-dimension, if 2^{nd} order basis and $\mathbf{g}^T = [1, 0, 2\beta]$ are used in the construction of $\tilde{\Phi}_a$ in (30), we have the following property:

$$\tilde{\varepsilon}(\mathbf{x}) = \sum_{I=1}^{NP} \tilde{\Phi}(\mathbf{x}; \mathbf{x} - \mathbf{x}_I) \varepsilon(\mathbf{x}_I) \approx \varepsilon(\mathbf{x}) + \beta \varepsilon_{,xx}(\mathbf{x}) \quad (32)$$

Recalling strain smoothing equation (24), and introducing approximation of displacements, we obtain

$$\begin{aligned} \tilde{\varepsilon}(\mathbf{x}) &= \sum_{I=1}^{NP} \tilde{\Phi}_a(\mathbf{x}; \mathbf{x} - \mathbf{x}_I) \varepsilon(\mathbf{x}_I) \\ &= \sum_{I=1}^{NP} \tilde{\Phi}_a(\mathbf{x}; \mathbf{x} - \mathbf{x}_I) \left\{ \frac{1}{2} \left[\frac{\partial u_i^h(\mathbf{x}_I)}{\partial x_j} + \frac{\partial u_j^h(\mathbf{x}_I)}{\partial x_i} \right] \right\} \\ &= \sum_{J=1}^{NP} \left(\tilde{B}_{iJ} d_{jJ} + \tilde{B}_{jJ} d_{iJ} \right) \end{aligned} \quad (33)$$

where

$$\tilde{B}_{iJ} = \sum_{I=1}^{NP} \frac{1}{2} \tilde{\Phi}_a(\mathbf{x}; \mathbf{x} - \mathbf{x}_I) \frac{\partial \Psi_J(\mathbf{x}_I)}{\partial x_i} \quad (34)$$

A one-dimensional damage mechanics problem as shown in figure 8 is analyzed. A rod with imperfection in the middle of the bar is subjected to a uniaxial tensile deformation as shown in figure 8. The equilibrium equation of this problem is

$$\begin{aligned} [E(1-D)\varepsilon]_{,x} &= 0, & 0 < x < L \\ u(0) &= 0 \\ u(L) &= g \end{aligned} \quad (35)$$

where D is the damage function. Here, we consider the following damage function:

$$D(\varepsilon) = \begin{cases} \frac{\varepsilon_c(\varepsilon - \varepsilon_i)}{\varepsilon(\varepsilon_c - \varepsilon_i)} & \text{if } \varepsilon_i \leq \varepsilon \leq \varepsilon_c \\ 1 & \text{if } \varepsilon > \varepsilon_c \end{cases} \quad (36)$$

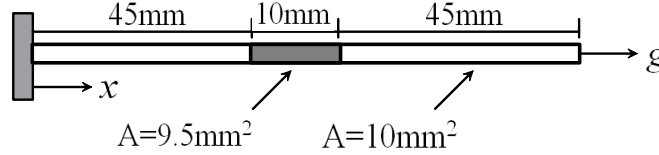


Figure 8. One-dimensional bar model.

Equations (35) and (36) represent a linear softening behavior as shown in figure 9.

The following parameters are used: $\varepsilon_i = 1.0 \times 10^{-4}$, $\varepsilon_c = 6.25 \times 10^{-3}$, and $E = 2 \times 10^6 N/mm^2$. An imperfection of the cross sectional area between $x = 30$ mm and $x = 40$ mm is introduced to initiate bifurcation from a homogeneous state of deformation. It is expected that the strain will localize in the imperfection zone, while the rest of the structure will relax elastically. We consider a second order gradient regularization $\tilde{\varepsilon} = \varepsilon + \beta \varepsilon_{,xx}$, with $\beta = 0.0408$, and third order basis functions are employed in the smoothing function. The force-displacement curves obtained using four spatial discretizations regularized with the second order gradient method shown in figure 10 demonstrate

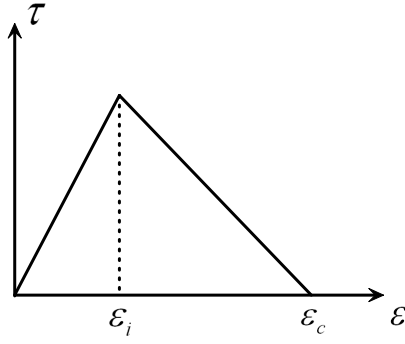


Figure 9. Linear softening stress-strain relation of 1-D elastic damage model.

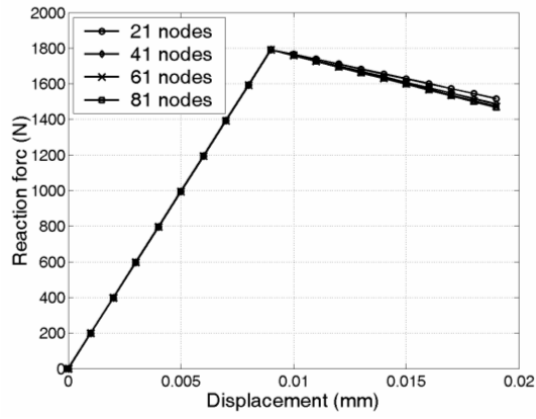


Figure 10. Force-displacement curves obtained by second order strain gradient method.

a mesh-independent results using the proposed method.

The regularized strain approximation in (33)-(34) also provides a stabilization to the nodally integrated discrete differential operator. Consider the weak form with the smoothed strain as follows:

$$\tilde{a}(\mathbf{v}^h, \mathbf{u}^h) = (\mathbf{v}^h, \mathbf{b}) + (\mathbf{v}^h, \mathbf{h})_{\partial\Omega^h_i} \quad (37)$$

where

$$\tilde{a}(\mathbf{v}^h, \mathbf{u}^h) = \int_{\Omega} \tilde{\boldsymbol{\varepsilon}}(\mathbf{v}^h) : \mathbf{C} : \tilde{\boldsymbol{\varepsilon}}(\mathbf{u}^h) d\Omega \quad (38)$$

The nodal integration of (38) yields:

$$\tilde{a}^h(\mathbf{v}^h, \mathbf{u}^h) = \sum_{L=1}^{NP} \tilde{\boldsymbol{\varepsilon}}(\mathbf{v}^h)_L : \mathbf{C} : \tilde{\boldsymbol{\varepsilon}}(\mathbf{u}^h)_L w_L \quad (39)$$

Note that by using the gradient producing properties in (31), we have:

$$\begin{aligned} & \tilde{a}^h(\mathbf{v}^h, \mathbf{u}^h) \\ &= \sum_{L=1}^{NP} \tilde{\boldsymbol{\varepsilon}}(\mathbf{v}^h)_L : \mathbf{C} : \tilde{\boldsymbol{\varepsilon}}(\mathbf{u}^h)_L w_L \\ &\approx \sum_{L=1}^{NP} \left[\boldsymbol{\varepsilon}(\mathbf{v}^h)_L + \sum_{i,j} \beta_{ij} D_{ij} \boldsymbol{\varepsilon}(\mathbf{v}^h)_L \right] : \mathbf{C} : \left[\boldsymbol{\varepsilon}(\mathbf{u}^h)_L + \sum_{i,j} \beta_{ij} D_{ij} \boldsymbol{\varepsilon}(\mathbf{u}^h)_L \right] w_L \end{aligned} \quad (40)$$

This is analogous to the use of Taylor expansion of gradient matrix in the stiffness matrix as a stabilization of the one-point integrated stiffness matrix [11] in finite element.

Figure 11 shows the comparison of the first nonzero eigenmodes of a nodally integrated stiffness matrix of 2-dimensional elasticity obtained using SCNI from (9), modified SCNI (M-SCNI) from (19), and gradient SCNI (G-SCNI) from (40), and no spurious oscillation is observed in M-SCNI and G-SCNI.

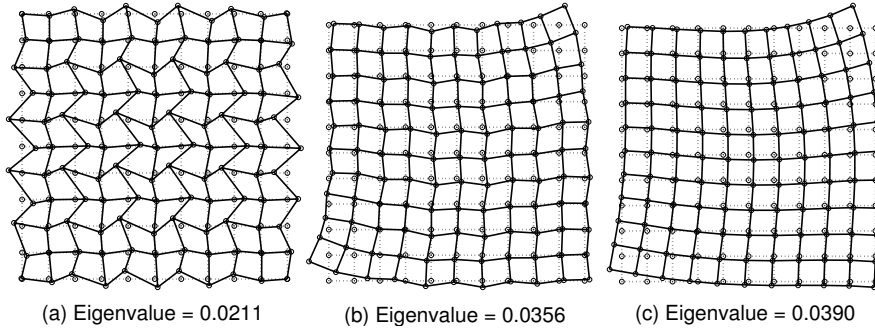


Figure 11. The first nonzero energy eigenmodes of nodally integrated stiffness using (a) SCNI, (b) M-SCNI, and (c) G-SCNI.

5 Application to Fragment Penetration Problems

5.1 Stabilized Nonconforming Nodal Integration(SNNI)

In transient large deformation problems, consider the following governing equation:

$$\rho \ddot{\mathbf{u}} = \nabla \cdot \boldsymbol{\tau} + \mathbf{b} \text{ in } \Omega_{\mathbf{x}} \quad (41)$$

with boundary conditions $u_i = g_i$ on $\Gamma_{\mathbf{x}}^g$ and $\tau_{ij}n_j = h_i$ on $\Gamma_{\mathbf{x}}^{h_i}$, where $\Omega_{\mathbf{x}}$, $\Gamma_{\mathbf{x}}^g$, and $\Gamma_{\mathbf{x}}^{h_i}$ are the domain, Dirichlet boundary, and Neumann boundary at the current configuration, respectively, ρ is density, $\boldsymbol{\tau}$ is Cauchy stress, \mathbf{b} is the body force vector, h_i is the traction. The corresponding Galerkin approximation is

$$(\mathbf{v}^h, \rho \mathbf{u}^h) + a(\mathbf{v}^h, \mathbf{u}^h) = (\mathbf{v}^h, \mathbf{b}) + (\mathbf{v}^h, \mathbf{h})_{\partial\Omega^{h_i}} \quad (42)$$

For fragment problems, updated Lagrangian formulation is employed, and the above weak form is integrated over the domain and boundary at the current configuration, in which $a(\mathbf{v}^h, \mathbf{u}^h)$ is expressed as:

$$a(\mathbf{v}^h, \mathbf{u}^h) = \int_{\Omega_x} \nabla^s \mathbf{v}^h : \boldsymbol{\tau}(\nabla^s \mathbf{u}^h) d\Omega \equiv \int_{\Omega_x} \boldsymbol{\varepsilon}(\mathbf{v}^h) : \boldsymbol{\tau}(\boldsymbol{\varepsilon}(\mathbf{u}^h)) d\Omega \quad (43)$$

where Ω_x is the domain at the current configuration, and

$$\boldsymbol{\varepsilon}(\mathbf{u}^h)_{ij} \equiv (\nabla^s \mathbf{u}^h)_{ij} = \frac{1}{2} \left(\frac{\partial u_i^h}{\partial x_j} + \frac{\partial u_j^h}{\partial x_i} \right) \quad (44)$$

and x_i is the spatial coordinate at the current configuration. In updated Lagrangian formulation, the approximation of \mathbf{u}^h is formulated at the current configuration [3], and constructing Voronoi cell for conforming strain smoothing in SCNI becomes tedious, and sometimes impossible during the fragmentation processes. To simplify the conforming strain smoothing in SCNI, we consider the following stabilized nonconforming nodal integration (SNNI), in which a simple nonconforming circular smoothing domain ϖ_L with boundary $\partial\varpi_L$ is used, as shown in figure 12. For elasticity, a nonconforming strain smoothing is introduced

$$\bar{\boldsymbol{\varepsilon}}_{ij}^h(\mathbf{x}_L) = \frac{1}{2\pi r^2} \int_{\varpi_L} (u_{i,j}^h + u_{j,i}^h) d\Omega = \frac{1}{2\pi r^2} \int_{\partial\varpi_L} (u_i^h n_j + u_j^h n_i) d\Gamma \quad (45)$$

where r is the radius of the circular smoothing domain.

Remark 1. Additional stabilization in the construction of stiffness follows (19), where $\boldsymbol{\varepsilon}(\mathbf{u}^h)_L^K$ can be evaluated at the centroid of the quarter circle associated with node L .

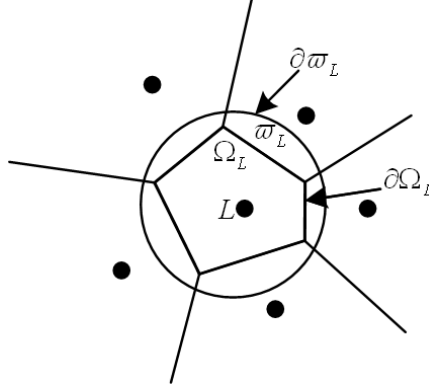


Figure 12. Averaging domain for SNNI.

5.2 Test of Convergence Property of SNNI in Elastostatics

A cantilever beam as shown in figure 6 is analyzed, where $L = 10m$, $H = 2m$, $P = 1.0 \times 10^4 N$, $E = 2.11 \times 10^7 Pa$, $\nu = 0.3$. The meshfree discretization (of half the beam) and the corresponding Voronoi nodal representative domain for SCNI and smoothing domain for SNNI with $\alpha = 1.5$ are shown in figure 13(a) and figure 13(b), where $\alpha = \sqrt{\int_{\varpi_L} d\Omega} / \sqrt{\int_{\Omega_L} d\Omega}$. Since this beam geometry has large surface to volume ratio, we do not add the additional stabilization in SNNI. The tip displacement normalized by the analytical solution is shown in table 1. The comparison of L_2 error norms of the solution obtained with various integration methods are compared in figure 14. The numerical experiment shows that the smoothing domain with α around 1.0 gives the best convergence rate for SNNI and is used for the following fragment problem. Although SNNI method offers a slight reduction in the solution accuracy compared to that of SCNI, the simplicity in the strain smoothing makes it particularly attractive for fragment problems. For problems that exhibit excessive particle motion and large degree of material separation, SNNI is the obvious choice over SCNI.

Integration Method	Accuracy (%)
Gauss 5×5	95.0
Direct Nodal	192.8
SCNI	99.2
SNNI	98.5

Table 1. Accuracy of tip displacement of beam problem by different integration techniques.

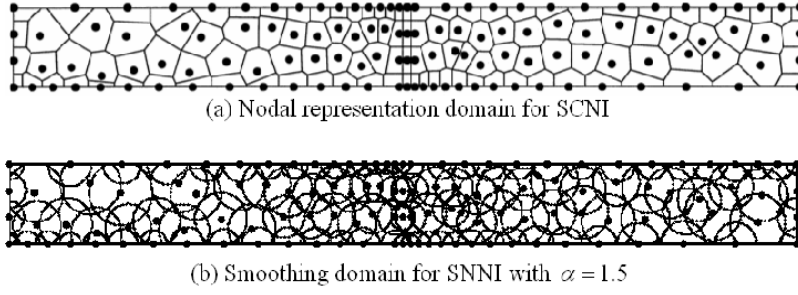


Figure 13. Nodal representative and smoothing domains for SCNI and SNNI.

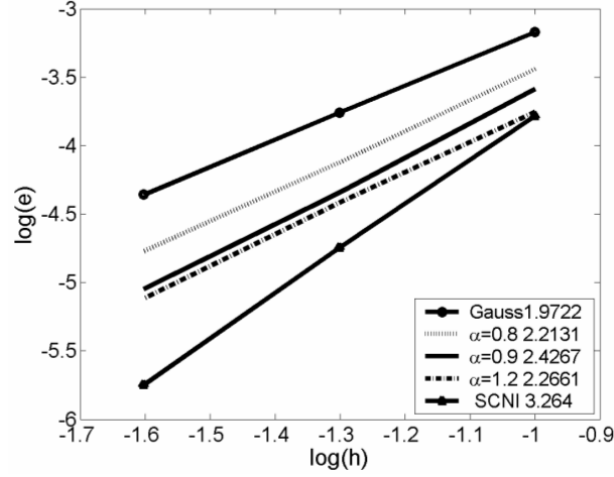


Figure 14. L_2 error norms of solution obtained from SNNI ($e = \|\mathbf{u}^h - \mathbf{u}\|_0$) with various α values, SCNI, and Gauss integration.

5.3 High Velocity Penetration

A Carbon-Tungsten projectile ball is impacting on a $0.4m \times 1m$ concrete wall. Plane strain assumption is assumed. The material constants of the ball are: Young's modulus $E = 630GPa$, Poisson's ratio $\nu = 0.33$, density $\rho = 8700kg/m^3$, initial yield stress $\sigma_y = 800MPa$ and the initial velocity of the ball is $500m/s$. The ball is discretized into 100 particles. The material constants of the concrete wall are: Young's modulus $E = 30GPa$, Poisson's ratio $\nu = 0.2$, density $\rho = 2400kg/m^3$, initial yield stress $\sigma_y = 40MPa$. The wall is fixed at both vertical ends and uniformly discretized into $41 \times 17 = 697$ particles. The two vertical surfaces of the concrete wall are fixed. The SNNI domain integration is employed. The progressive deformation of the penetration is shown in figure 15.

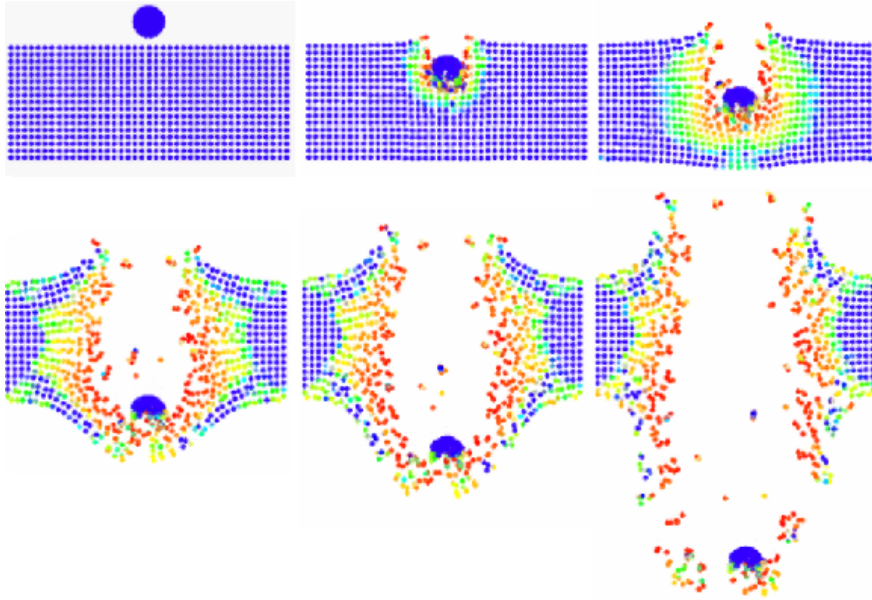


Figure 15. Progressive deformation in high velocity penetration.

6 Conclusions

In this paper, we have introduced several forms of strain smoothing for stabilization and regularization of numerical instability resulting from nodal integration of meshfree Galerkin weak form and material instability due to strain softening and localization. In many large deformation and fragment penetration problems, nodal integration in meshfree methods is highly desirable for the ability to trace complex material motion and for computational efficiency. Nodal integration, however, yields spatial instability. Conforming strain smoothing in stabilized conforming nodal integration (SCNI) has been introduced to stabilize spurious zero energy modes. This study demonstrated that SCNI does not guarantee coercivity. The energy of an oscillatory mode can be very small and spurious nonzero energy modes can exist as the mesh is refined. To recover coercivity, an additional stabilization has been added to the SCNI with a rather simple construction. Test problems have been analyzed to examine the stability and convergence of the modified SCNI method.

In the event of strain softening and localization, the change of sign in the tangent moduli yields an ill-posed problem and requires a regularization for unique solution. The classical gradient type regularization operating on strain results in a governing equation with higher order differentiation, and thus requires additional nonphysical boundary conditions for a solution. This strain gradi-

ent regularization can be implicitly imbedded in a gradient reproducing kernel strain smoothing, leading to a naturally regularized weak form without the need of additional nonphysical boundary conditions. It is shown in the numerical test that the imbedded gradient term in the gradient strain smoothing offers a stabilization to the nodally integrated stiffness matrix similar to the stabilization obtained from Taylor series expansion of the one-point evaluated gradient matrix in finite element [11].

For application to fragment and penetration problems, the construction of Voronoi cells in the conforming strain smoothing in SCNI is too tedious and sometimes impossible. We have introduced a stabilized nonconforming nodal integration (SNNI) in which a nonconforming circular strain smoothing zone has been employed. It is shown that although the conforming property is relaxed in SNNI strain smoothing which results in a slight reduction in the solution accuracy compared to that of SCNI, the simplicity in the nonconforming strain smoothing makes it particularly attractive for fragment penetration problems.

References

1. S. Beissel and T. Belytschko, *Nodal integration of the element-free Galerkin method*, Computer Methods in Applied Mechanics and Engineering **139** (1996), 49–74.
2. J. Bonet and S. Kulasegaram, *Correction and stabilization of smooth particle hydrodynamics methods with applications in metal forming simulation*, International Journal for Numerical Methods in Engineering **47** (1999), 1189–1214.
3. J. S. Chen, C. Pan, C. T. Wu, and W. K. Liu, *Reproducing Kernel Particle Methods for Large Deformation Analysis of Nonlinear Structures*, Computer Methods in Applied Mechanics and Engineering **139** (1996), 195–227.
4. J. S. Chen, C. T. Wu, and T. Belytschko, *Regularization of Material Instabilities by Meshfree Approximation with Intrinsic Length Scales*, International Journal for Numerical Methods in Engineering **47** (2000), 1303–1322.
5. J. S. Chen, C. T. Wu, S. Yoon, and Y. You, *A Stabilized Conforming Nodal Integration for Galerkin Meshfree Methods*, International Journal for Numerical Methods in Engineering **50** (2001), 435–466.
6. J. S. Chen, C. T. Wu, S. Yoon, and Y. You, *Nonlinear Version of Stabilized Conforming Nodal Integration for Galerkin Meshfree Methods*, International Journal for Numerical Methods in Engineering **53** (2002), 2587–2615.
7. J. S. Chen, X. Zhang, and T. Belytschko, *An Implicit Gradient Model by a Reproducing Kernel Strain Regularization in Strain Localization Problems*, Computer Methods in Applied Mechanics and Engineering **193** (2004), 2827–2844.
8. R. De Borst, and J. Pamin, *Gradient plasticity in numerical simulation of concrete cracking*, Eur. J. Mech. A/Solids **15** (1996), 295–3202.
9. R. De Borst, R. H. Pamin, R. H.J. Peerlings, and L. J. Sluys, *On Gradient-enhanced Damage and Plasticity Models for Failure in Quasi-brittle and Frictional Materials*, Computational Mechanics **17** (1996), 130–141.

10. D. Lasry, and T. Belytschko, *Localization Limiters in Transient Problems*, Int. J. of Solids and Struct. **24** (1988), 581–597.
11. W. K. Liu, J. S.J. Ong, and R. A. Uras, *Finite element stabilization matrices-a unification approach*, Computer Methods in Applied Mechanics and Engineering **53** (1985), 13–46.
12. P. W. Randles, and L. D. Libersky, *Normalized SPH with stress points*, International Journal for Numerical Methods in Engineering **48** (2000), 1445–1462.
13. D. Wang, and J. S. Chen, *Locking Free Stabilized Conforming Nodal Integration for Meshfree Mindlin-Reissner Plate Formulation*, Computer Methods in Applied Mechanics and Engineering **193** (2004), 1065–1083.
14. J. W. Yoo, B. Moran, and J. S. Chen, *Stabilized Conforming Nodal Integration in the Natural-Element Method*, International Journal for Numerical Methods in Engineering **60** (2004), 861–890.